第 34 卷第 6 期 无 机 化 学 学 报 Vol.34 No.6
2018 年 6 月 CHINESE JOURNAL OF INORGANIC CHEMISTRY 1173-1182

核壳结构的 Co_3O_4@δ-MnO_2/Pt 作为锂氧电池高效催化正极

成 浩[1] 谢 健*,[1,2] 陈 振[3] 涂 健[3] 曹高劭[2] 赵新兵[1,2]
([1]浙江大学材料科学与工程学院,杭州 310027)
([2]浙江省电池新材料与应用技术研究重点实验室,杭州 310027)
([3]湖南立方新能源科技有限责任公司,株洲 412000)

摘要:通过简易、可控的水热方法在泡沫镍基体上直接生长了核壳结构的阵列型 Co_3O_4@δ-MnO_2/Pt 正极。阵列电极有利于电极的润湿、氧气的传输和 Li_2O_2 的负载。Co_3O_4@δ-MnO_2/Pt 正极对氧还原和氧析出反应具有高的催化性能,可促使 Li_2O_2 依附 Co_3O_4@δ-MnO_2/Pt 阵列生长,从而保持阵列结构。该生长行为有利于 Li_2O_2 在充电时分解。以 Co_3O_4@δ-MnO_2/Pt 为催化正极的锂氧电池显示出高的容量(在电流密度 100 mA·g^{-1} 时容量为 2 480 mAh·g^{-1}),以及长的循环寿命(容量限定在 500 mAh·g^{-1} 时,在 200 mA·g^{-1} 电流密度下,可循环 65 次),该性能超过了使用 Co_3O_4 或 Co_3O_4@δ-MnO_2 催化剂的电池。

关键词:锂氧电池;电催化;核壳阵列;Co_3O_4@δ-MnO_2/Pt
中图分类号:TQ152;TM911 **文献标识码**:A **文章编号**:1001-4861(2018)06-1173-10
DOI:10.11862/CJIC.2018.137

Co_3O_4@δ-MnO_2/Pt Core-Shell Arrays as Efficient Catalytic Cathode for Lithium-Oxygen Cells

CHENG Hao[1] XIE Jian*,[1,2] CHEN Zhen[3] TU Jian[3] CAO Gao-Shao[2] ZHAO Xin-Bing[1,2]
([1]*School of Materials Science and Engineering, Zhejiang University, Hangzhou* 310027, *China*)
([2]*Key Laboratory of Advanced Materials and Applications for Batteries of Zhejiang Province, Hangzhou* 310027, *China*)
([3]*LI-FUN Technology Corporation Limited, Zhuzhou, Hunan* 412000, *China*)

Abstract: A unique core-shell Co_3O_4@δ-MnO_2/Pt arrays-type cathode on Ni foam has been fabricated by a facile, controlled hydrothermal approach. The array-type structure facilitates the electrode wetting and oxygen gas transport and supplies free volume for Li_2O_2 loading. The Co_3O_4@δ-MnO_2/Pt cathode exhibits high catalytic effect for ORR and OER, where thin-layered Li_2O_2 shows conformal growth along the surface of the Co_3O_4@δ-MnO_2/Pt arrays with the array-type structure remained. This growth behavior of Li_2O_2 renders easy decomposition of Li_2O_2 upon charge. Li-O_2 cells with Co_3O_4@δ-MnO_2/Pt delivers a high discharge capacity (2 480 mAh·g^{-1} at 100 mA·g^{-1}) and long cycle life (65 cycles at 200 mA·g^{-1} with a limited capacity of 500 mAh·g^{-1}), which are better than those with Co_3O_4 or Co_3O_4@δ-MnO_2 cathodes.

Keywords: Li-O_2 cells; electrocatalysis; core-shell array; Co_3O_4@δ-MnO_2/Pt

Lithium-oxygen (Li-O_2) batteries now have captured a world-wide attention due to the extremely high theoretical energy density of 3 505 Wh·kg^{-1}, showing promising applications in electric vehicles[1-10]. In nonaqueous Li-O_2 batteries, during discharge, oxygen is reduced to O^{2-} which reacts with Li^+ to form Li_2O_2 at

收稿日期:2018-01-09。收修改稿日期:2018-03-23。
国家自然科学基金(No.51572238)和湖南省战略新兴产业计划(No.2016GK4030)项目资助。
*通信联系人。E-mail:xiejian1977@zju.edu.cn

cathode. Upon the subsequent recharge, Li_2O_2 can be electrochemically decomposed to release oxygen and Li^+[4]. Unlike the shuttle mechanism in Li-ion batteries, the deposition of insulating/insoluble Li_2O_2 will cause sluggish oxygen reduction/evolution reaction (ORR/OER) kinetics, leading to high polarization, low yieldable capacity and poor cycling stability[11-12]. It is widely acknowledged that the electrode kinetics can be enhanced by using efficient catalysts. Besides the components, the architecture of catalytic electrode should also be specially designed to adapt the Li_2O_2 deposition without drastically changing the structure of the electrodes[13-17].

Carbon materials have been widely used as the catalysts for Li-O_2 batteries due to the low cost, high electronic conductivity, light weight and easy manipulation of the porosity[18-23]. However, carbon materials suffer from decomposition chemically or electrochemically in contact with Li_2O_2 or LiO_2[24-25]. In addition, the catalytic performance of carbon materials for OER is not satisfactory. Although noble metals provide the best catalytic activity for both ORR and OER[26-33], the high cost limits their large-scale applications. Transition metals oxides, such as MnO_2, Co_3O_4, NiO, and CoOOH, are suitable due to low cost, structural stability and relatively high catalytic activity for ORR/OER[34-42]. Thus, a compromise can be made by combining transition metals oxides and noble metals. However, unlike carbon materials, it is difficult to allocate free space for Li_2O_2 deposition in oxides.

Array-type electrode prepared by direct growth route is desirable since the voids between the arrays could be used to store Li_2O_2[37,41,43-46]. Cui et al.[37] first report a Co_3O_4-array-catalyzed Li-O_2 cell with low polarization and high capacity. The work by Chang et al.[43] show that Li-O_2 cell could sustain stable cycling up to 300 times at 500 $mAh \cdot g^{-1}$ when using a carbon/binder-free RuO_x/TiN nanotube arrays cathode. Recent report by Liu et al.[44] show that Li-O_2 batteries with TiO_2-array cathode demonstrate long cycle life, superior rate capability, high round-trip efficiency, and good recoverability of the catalytic electrode. For the array-type electrode, realizing conformal growth of Li_2O_2 on the arrays is desirable to retain the voids between the arrays and keep intimate contact between Li_2O_2 and catalyst. Nevertheless, as previously reported, conformal growth of insulating Li_2O_2 will easily deactivate the catalyst with low capacity due to blocked electron transport[47-50].

In this work, we design a unique core-shell Co_3O_4@δ-MnO_2/Pt arrays-type electrode on nickel foam by a controllable, facile route as binder-free electrodes for Li-O_2 cells, where the Co_3O_4 acts as the "core" and ultrathin δ-MnO_2 nanosheets with Pt as the "shell". MnO_2 was selected because of its high catalytic activity for ORR/OER[34-36,51]. Co_3O_4 acts both as the catalytically active component and as the substrate for MnO_2 deposition. The decoration of Pt not only enhances the catalytic activity but also guides conformal growth of Li_2O_2. The advantages of this electrode design include: (1) the array-type structure facilitates the electrode wetting by electrolyte and O_2 transport and supplies large room for Li_2O_2 loading; (2) the conformal growth of thin-layered Li_2O_2 on Co_3O_4@δ-MnO_2/Pt enables its easy decomposition upon charge; (3) the porous structure of δ-MnO_2 assures high Li_2O_2 loading despite the conformal growth mode; (4) the side reactions related to binder and conductive agent are totally precluded or largely reduced due to binder- and conductive-agent-free electrode configuration. As a result, Li-O_2 cells with core-shell Co_3O_4@δ-MnO_2/Pt arrays exhibit high capacity and long cycle life.

1 Experimental

1.1 Electrode preparation

Co_3O_4@δ-MnO_2/Pt arrays-type electrodes were synthesized by three steps. First, Co_3O_4 nanowire arrays on Ni foam substrate were prepared by a facile hydrothermal route. $Co(NO_3)_2 \cdot 6H_2O$ (1.2 mmol), NH_4F (1.2 mmol), and urea (3 mmol) were dissolved into 50 mL of deionized (DI) water under vigorous stirring. The solution was then transferred into a Teflon-lined stainless steel autoclave with a piece of Ni foam immersed. The autoclave was sealed and heated in an electric oven at 120 ℃ for 5 h. After being cooled to

room temperature, the Ni foam piece with a pink deposit was collected, washed with DI water and absolute ethanol several times, and dried at 60 ℃ in air overnight. The product was further heated at 400 ℃ for 2 h in air to obtain Ni-supported Co_3O_4 (Co_3O_4/Ni). For the growth of δ-MnO_2 in the second step, a piece of Co_3O_4/Ni was first immersed into a 0.04 mol·L^{-1} aqueous solution of glucose for 24 h, followed by carbonization at 450 ℃ in Ar for 2 h. After that, 80 mg $KMnO_4$ (99.5%, Sinopharm Chemical Reagent Co., Ltd.) was dissolved in 60 mL of DI water with vigorous stirring to form a homogeneous solution. The carbon modified Co_3O_4/Ni was soaked in the above solution for 1.5 h. Afterwards, the mixture was transferred into a Teflon-lined stainless steel autoclave and heated at 85 ℃ for 2.5 h. After cooling down to room temperature naturally, the Ni foam with a brown deposit was collected and washed repeatedly with DI water and absolute ethanol. The electrode was then dried at 60 ℃ in air overnight followed by heating at 300 ℃ in Ar for 2 h to obtain Ni-supported core-shell Co_3O_4/δ-MnO_2. Finally, for the platinum deposition, $H_2PtCl_6 \cdot 6H_2O$ was dispersed in DI water at a concentration of 0.24 mg·mL^{-1} under stirring, a piece of Ni-supported Co_3O_4@δ-MnO_2 was soaked in the above solution overnight. The electrode was then dried at 60 ℃ in air for 5 h followed by heating at 300 ℃ in Ar for 2 h to get Ni-supported Co_3O_4@δ-MnO_2/Pt. The total loading of Co_3O_4@δ-MnO_2/Pt on Ni substrate is around 1.4 mg·cm^{-2} and Pt loading is around 0.2 mg·cm^{-2}.

1.2 Electrode characterization

X-ray diffraction (XRD) patterns of the electrodes were acquired using a Rigaku D/Max-2550pc powder diffractometer equipped with Cu $K\alpha$ radiation (λ= 0.154 1 nm). The operating voltage and current were 40 kV and 250 mA, respectively, and 2θ=10°~80°. The morphologies of the pristine and cycled electrodes were observed by field-emission scanning electron microscopy (SEM) using an S-4800 microscope (Hitachi, Japan) at an accelerating voltage of 5 kV. Transmission electron microscopy (TEM) and high-resolution TEM (HRTEM) were conducted on a JEM 2100F microscope at an accelerating voltage of 200 kV. X-ray photoelectron spectra (XPS) of the discharged and charged electrodes were collected on a KRATOS AXIS ULTRA-DLD spectrometer with Al $K\alpha$ radiation ($h\nu$=1 486.6 eV). To analyze the cycled electrodes by SEM, TEM and XPS, the electrodes or electrode components were carefully handled before the various *ex-situ* characterizations[52].

1.3 Electrochemical measurements

Coin-type Li-O_2 cells were assembled in the Ar-filled glovebox using lithium foil as the anode, Ni-supported Co_3O_4@δ-MnO_2/Pt as the cathode, and Celgard C480 membrane as the separator. The electrolyte was 1 mol·L^{-1} $LiClO_4$ (≥99.99%, Sigma-Aldrich) in tetraethylene glycol dimethyl ether (TEGDME). The cathodes were dried at 80 ℃ in vacuum overnight before cell assembly. The assembled cells were purged with pure O_2 for 20 min and stayed at open voltage circuit (OCV) for 5 h before the electrochemical tests. Charge and discharge cycling was performed on a Neware battery cycler (Shenzhen, China) in a voltage window of 2.0~4.5 V (vs Li/Li^+). The specific capacity (mAh·g^{-1}) and current density (mA·g^{-1}) of the cells were calculated based on the weight of Co_3O_4@δ-MnO_2/Pt. For the cells using Co_3O_4 and Co_3O_4@δ-MnO_2 catalysts, the specific capacity and current density were calculated based on the weight of Co_3O_4 and Co_3O_4@δ-MnO_2, respectively. Electrochemical impedance spectroscopy (EIS) measurements were conducted on the VersaSTAT3 electrochemistry workstation by applying an AC signal of 5 mV amplitude over the frequency range 10^{-2} to 10^5 Hz. All of the electrochemical tests were performed at 25 ℃.

2 Results and discussion

Fig.1a and the enlarged view (Fig.1b) show the XRD patterns of Co_3O_4 and Co_3O_4@δ-MnO_2/Pt supported on Ni foam. The three strong diffraction peaks at 44.5°, 51.8°, and 76.4° (2θ) are from the nickel substrate, and the presence of Co_3O_4 and Co_3O_4@δ-MnO_2/Pt is confirmed by XRD patterns in Fig.1b, while the presence of Pt is not detected in XRD due to the low content. The XRD shows that the MnO_2 is δ-MnO_2. In order to further confirm the existence of Pt, XPS

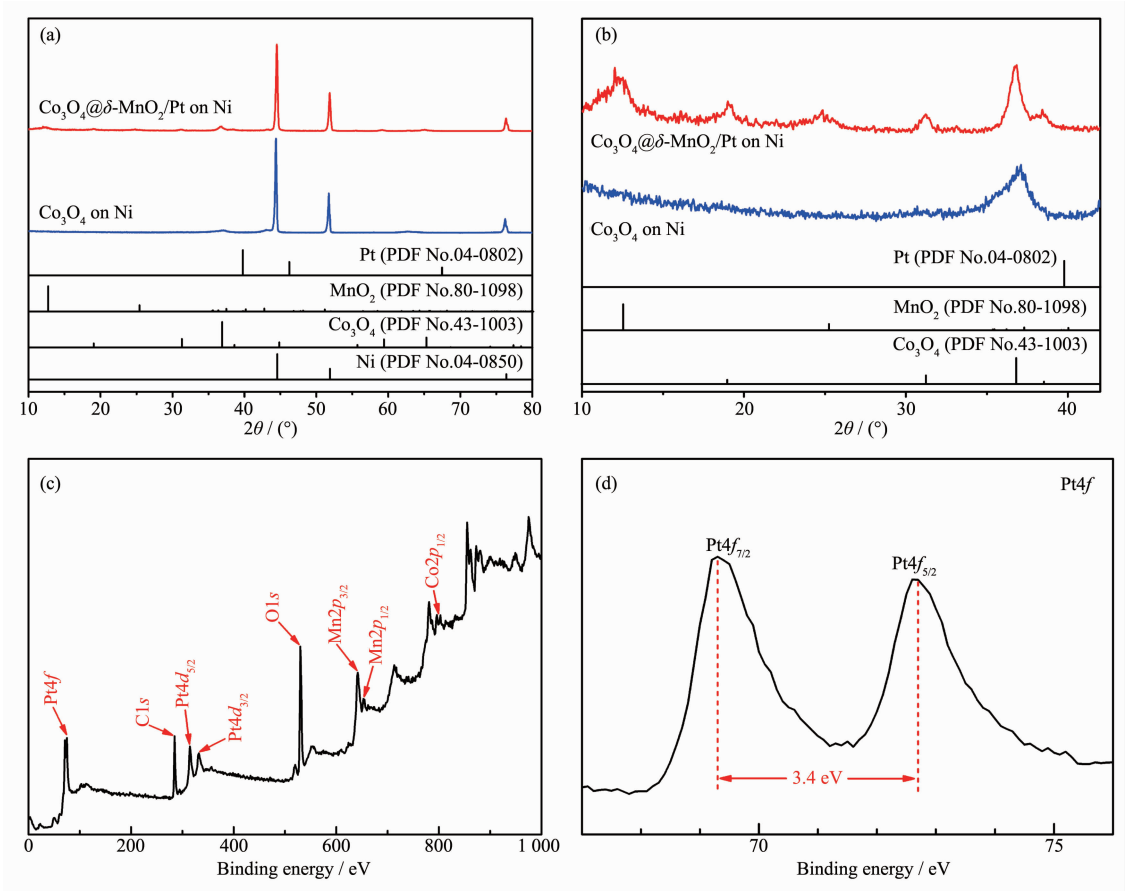

Fig.1 (a) XRD patterns of Co_3O_4 and Co_3O_4@δ-MnO_2/Pt on Ni foam; (b) Enlarged view in (a); (c) XPS survey spectrum and (d) Pt4*f* XPS spectrum of Co_3O_4@δ-MnO_2/Pt

analysis was performed. The survey spectrum in Fig. 1c reveals the presence of the expected O, Co, Mn and Pt elements. In Fig.1d, the bands at 69.3 and 72.7 eV correspond to the binding energy of Pt4$f_{7/2}$ and Pt4$f_{5/2}$, respectively[53]. In Fig.S1a, the peaks at 778.6 and 794.1 eV are the Co2*p* spectra of Co^{3+}, and the peaks at 780.3 and 796.0 eV are Co2*p* of Co^{2+} [54]. The bands at 639.8 and 651.4 eV (Fig.S1b) correspond to the binding energy of Mn2$p_{3/2}$ and Mn2$p_{1/2}$, in good accordance with the previous report[55].

The morphology and structural features of the prepared electrodes were characterized by SEM and TEM. Fig.2 shows the SEM images of Co_3O_4, Co_3O_4@δ-MnO_2, and Co_3O_4@δ-MnO_2/Pt at different magnifications. Note that Co_3O_4 nanowires grow uniformly on the skeletons of the Ni foam. The Co_3O_4 nanowires have a diameter below 200 nm and a length of several microns (Fig.2(a,b)). After the MnO_2 growth, thin MnO_2 nanosheets are uniformly covered on the whole surface of the Co_3O_4 nanowires, forming a core-shell porous structure as shown in Fig.2(c,d). As seen in Fig.2(e,f), the introduction of Pt does not change the morphology of core-shell Co_3O_4@δ-MnO_2 obviously with the array structure maintained. The pores in Pt/δ-MnO_2 and the voids between the arrays are beneficial to the electrolyte infiltration and oxygen gas transportation and provide the space for Li_2O_2 deposition. The Co_3O_4@δ-MnO_2/Pt was further characterized by TEM, HRTEM and energy dispersive X-ray spectroscopy (EDS) mapping as shown in Fig.3. The results confirm that Co_3O_4, δ-MnO_2 and Pt construct a uniform electrode, where Co_3O_4 exhibits a polycrystalline nanowire structure, δ-MnO_2 has a sheet-like shape and Pd nanocrystals have a small size below 20 nm. In Fig.3f, the lattice spacings of 0.46, 0.22 and 0.21 nm correspond to the planes of Co_3O_4 (111), Pt (111) and δ-MnO_2 ($\bar{1}$12), respectively. The above characterizations confirm the formation of Co_3O_4@δ-MnO_2/Pt.

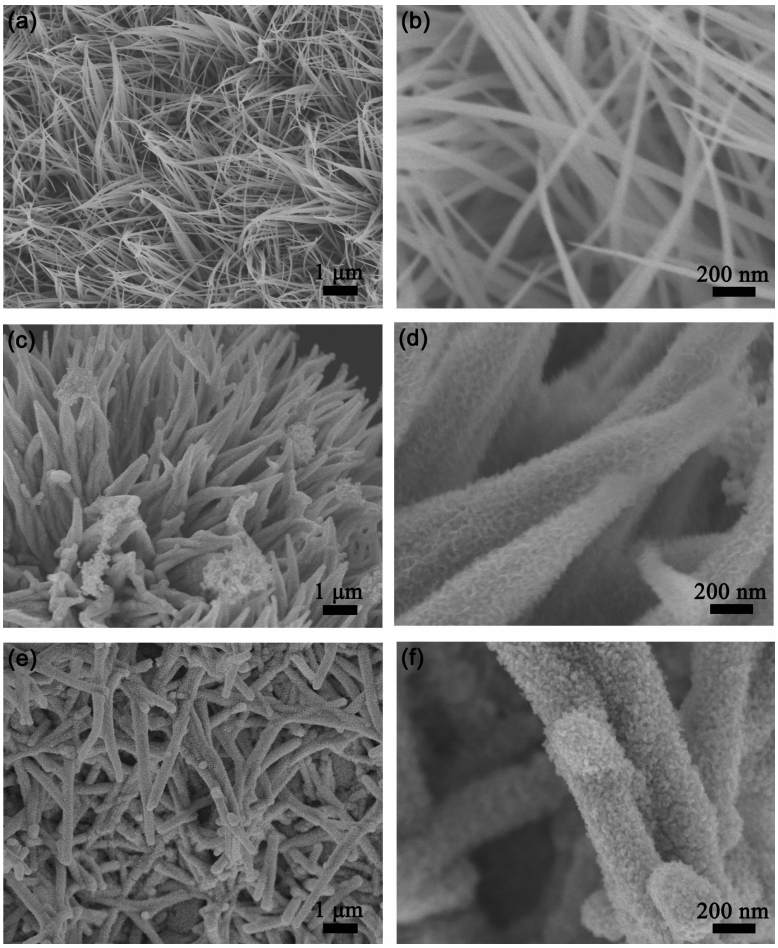

Fig.2　SEM images of (a, b) Co_3O_4, (c, d) Co_3O_4@δ-MnO_2, and (e, f) Co_3O_4@δ-MnO_2/Pt

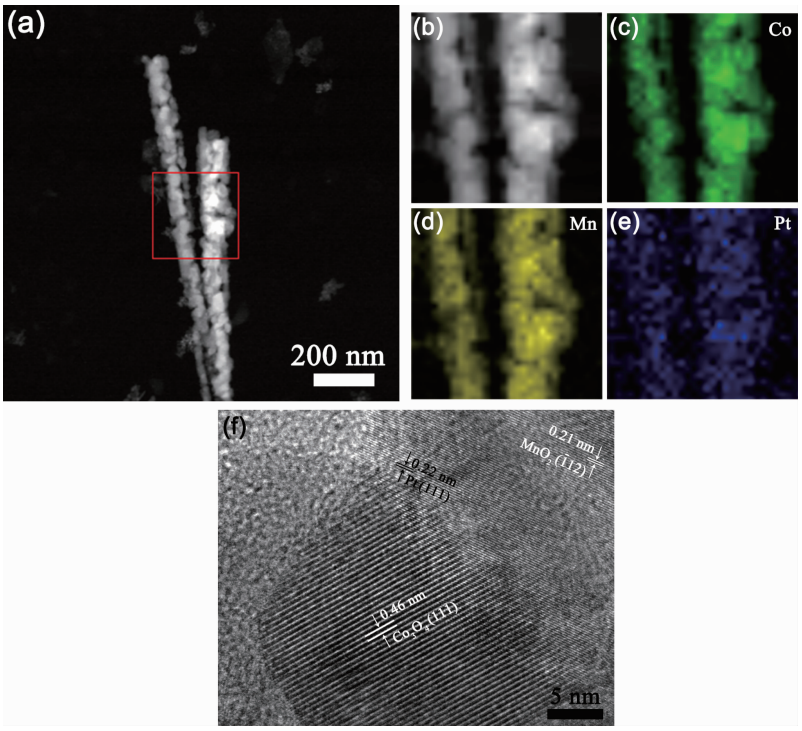

Fig.3　(a) Dark-field TEM image, (b~e) EDS mappings in the selected area and (f) HRTEM images of Co_3O_4@δ-MnO_2/Pt

The electrocatalytic activity of Co_3O_4@δ-MnO_2/Pt was investigated in Li-O_2 cells and compared with that of Co_3O_4 and Co_3O_4@δ-MnO_2. The current density and specific capacity were calculated by the total mass of catalyst on the Ni substrate. The cycling performance of the Co_3O_4, Co_3O_4@δ-MnO_2 and Co_3O_4@δ-MnO_2/Pt-catalyzed Li-O_2 cells was evaluated by galvanostatic cycling at 200 mA·g^{-1} between 2.0~4.5 V with a limited capacity of 500 mAh·g^{-1}. As shown in Fig.4(a, b), the cell with Co_3O_4@δ-MnO_2/Pt catalyst can sustain stable cycling for 65 cycles. While for the cells with Co_3O_4 and Co_3O_4@δ-MnO_2 catalytic cathodes, the cycling can last only 10 cycles and 28 cycles, respectively (Fig.4a and Fig.S2). To demonstrate the high catalytic activity of Co_3O_4@δ-MnO_2/Pt, the cell was also cycled at a higher limited capacity of 1 000 mAh·g^{-1} at a current density of 200 mA·g^{-1}. In this case, the stable cycling can still last 32 cycles (Fig.S3). It should noted that the electrode has a relatively high catalyst loading of about 1.4 mg·cm^{-2}. The cycling performance of the cell is better than or comparable with those with similar catalysts and same limited capacity[56-57]. The better cycle performance of the Li-O_2 cell with Co_3O_4@δ-MnO_2/Pt catalyst can be attributed to the unique microstructure and components of the cathode. Pt nanoparticles are highly efficient in catalyzing the ORR/OER in the air cathode[58], leading to enhanced formation/decomposition of Li_2O_2 and thereby long cycle life. In addition, the binder-free electrode design also contributes to good cycling stability of the cell with Co_3O_4@δ-MnO_2/Pt catalyst. Of note is that, the cell shows performance degradation after 60 cycles. This may result from factors such as decomposition of electrolyte or Li corrosion. A previous report show that Pt shows no selectivity in its catalytic activity toward Li_2O_2 oxidation reaction and electrolyte decomposition[31], which is also partly responsible for the limited cycle life.

Fig.4(c,d) show the discharge profiles of the Co_3O_4@δ-MnO_2 and Co_3O_4@δ-MnO_2/Pt-catalyzed Li-O_2 cells

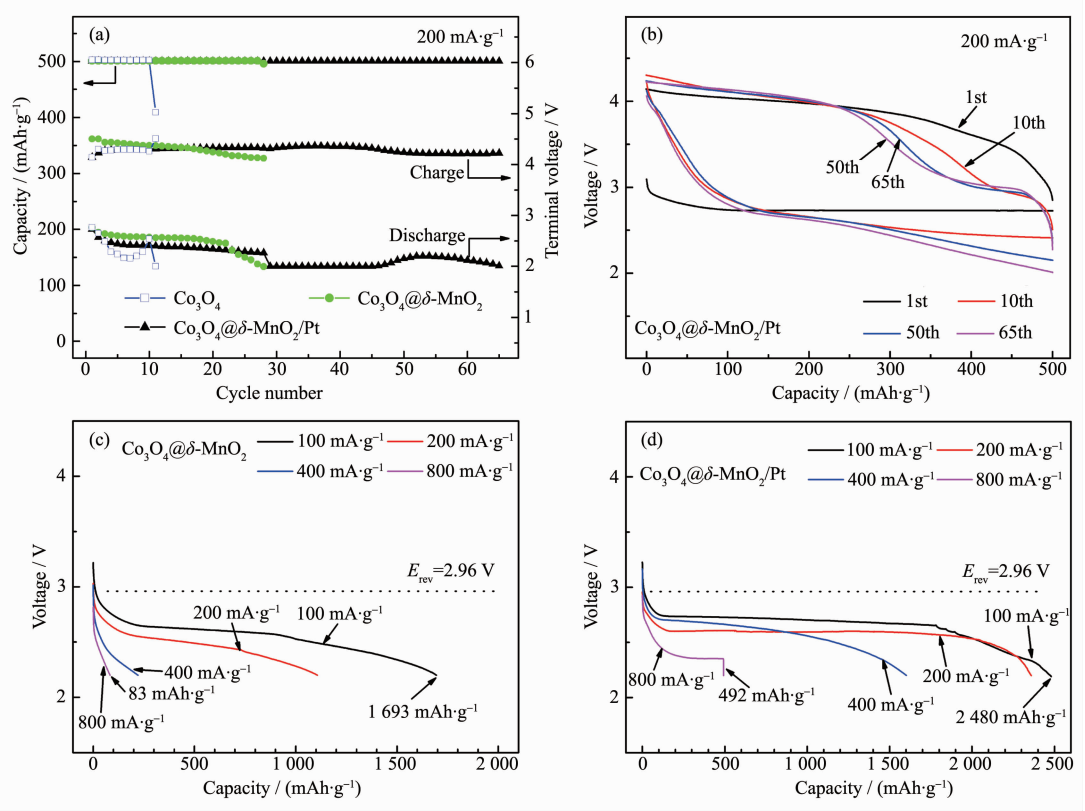

Fig.4 (a) Terminal voltages of Co_3O_4, Co_3O_4@δ-MnO_2 and Co_3O_4@δ-MnO_2/Pt-catalyzed Li-O_2 cells at a limited capacity of 500 mAh·g^{-1}; (b) Voltage profiles of Co_3O_4@δ-MnO_2/Pt-catalyzed Li-O_2 cell; Discharge profiles of (c) Co_3O_4@δ-MnO_2 and (d) Co_3O_4@δ-MnO_2/Pt-catalyzed Li-O_2 cells at various current densities

at various current densities. In the figures, E_{rev} is the reversible potential of Li-O_2 cells, namely, 2.96 V vs Li/Li^+. At 100 mA·g^{-1}, the cell with Co_3O_4@δ-MnO_2/Pt yields a capacity of 2 480 mAh·g^{-1} and exhibits a high discharge plateau of 2.71 V. When the current density increases from 100 to 800 mA·g^{-1}, the discharge capacity and plateaus decrease gradually. But even at 800 mA·g^{-1}, the cell could still deliver a capacity of 492 mAh·g^{-1} due to the excellent catalytic activity of Co_3O_4@δ-MnO_2/Pt for ORR. In comparison, the cell with Co_3O_4@δ-MnO_2 catalyst shows a lower capacity of 1 693 mAh·g^{-1} and a lower discharge plateau of 2.59 V at 100 mA·g^{-1}. The discharge capacity decreases rapidly to 83 mAh·g^{-1} when the current density increases to 800 mA·g^{-1}. The low capacity of the Co_3O_4@δ-MnO_2-catalyzed cell indicates its poor ORR catalytic activity. The obviously enhanced catalytic activity of Co_3O_4@δ-MnO_2/Pt is closely related to the introduction of Pt. It is expected that the presence of Pt will alter the crystallization behavior of Li_2O_2 by supplying catalytically active sites.

To clarify the superior catalytic activity of Co_3O_4@δ-MnO_2/Pt and the role that it plays in increasing the cycle performance of the cell, the electrodes after discharge were observed by SEM and TEM. The loading of the SEM/TEM holders to the chamber was finished as soon as possible to minimize the exposure of the samples to air. As shown in Fig.5(a,b), no large Li_2O_2 particles can be found on the discharged Co_3O_4@δ-MnO_2/Pt electrode, and the pristine array-type structure of Co_3O_4@δ-MnO_2/Pt was generally preserved after discharge to 500 mAh·g^{-1}. To reveal the growth position of Li_2O_2 on the electrode, the morphologies were observed and compared to the original Co_3O_4@δ-MnO_2/Pt. In the discharged electrodes, it seems that the Li_2O_2 forms inside the porous δ-MnO_2 and a fluffy

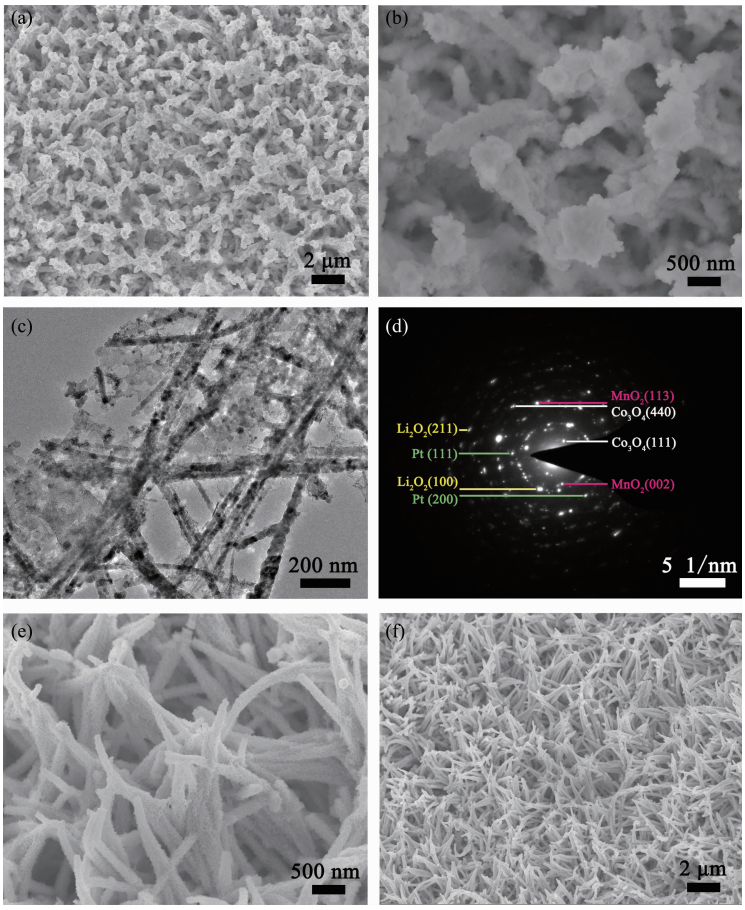

Cells were discharged and charged to 500 mAh·g^{-1} at 200 mA·g^{-1}

Fig.5　(a, b) SEM images, (c) TEM image and (d) SAED pattern of Co_3O_4@δ-MnO_2/Pt after the first discharge; (e, f) SEM images of Co_3O_4@δ-MnO_2/Pt after the first charge

substance grows conformally along the surface of the Co_3O_4@δ-MnO_2/Pt arrays, where the original array structure with voids is clearly visible. Namely, the pores in the pristine Co_3O_4@δ-MnO_2/Pt were filled by the Li_2O_2. This form of Li_2O_2 is usually rich in defects and poorly crystallized and thus easily to be decomposed[59]. The fluffy substance is further characterized by TEM (Fig.5c) and is confirmed to be Li_2O_2 by selected area electron diffraction (SAED, Fig.5d). From these results, it can be concluded that Co_3O_4@δ-MnO_2/Pt arrays catalyzes the conformal growth of thin-layered Li_2O_2 along the surface of electrode.

For the Co_3O_4@δ-MnO_2/Pt electrode, after recharge, the porous structure is visible again, indicative of sufficient decomposition of the discharge product (Fig.5e). Besides, the array-type structure of Co_3O_4@δ-MnO_2/Pt remains intact (Fig.5f). The reversible formation/decomposition of Li_2O_2 is confirmed by Li1*s* XPS (Fig.6a) and further supported by EIS measurements (Fig.6b and Table 1). In the Nyquist plots, the fitted curves are obtained by using the equivalent circuit in the inset, where R_e represents ohm resistance of cell components, R_f and Q_1 represent surface film resistance and relaxation capacitance, R_{ct} and Q_2 correspond to the charge transfer resistance and double-layer capacitance, and Z_w is associated with the bulk diffusion of Li ions. In the table, Y is admittance response of constant phase element Q_1 and Q_2 and n is index of the angular frequency [60]. The remarkable increase in R_{ct} (from 331.9 to 767.1 Ω) after discharge indicates the deposition of insulating Li_2O_2 which passivates the electrode, whereas the decrease in R_{ct} (from 767.1 to 301.6 Ω) denotes the sufficient removal of Li_2O_2 after recharge. From these results, it can be seen that the Ni-supported Co_3O_4@δ-MnO_2/Pt electrode is highly efficient in catalyzing ORR/OER by controlling the Li_2O_2 growth, which can explain the high discharge capacity and long cycle life of the cells.

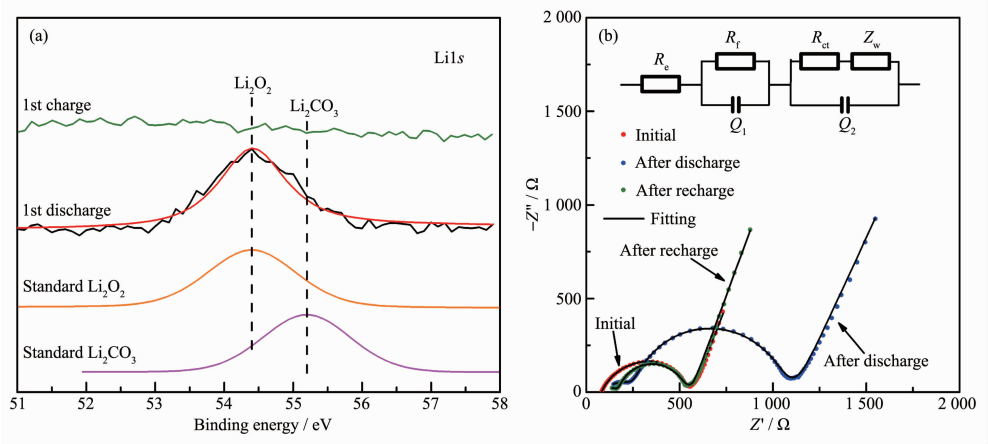

Fig.6 (a) Li1*s* XPS after the first cycle and (b) Nyquist plots and corresponding fittings of Li-O_2 cells with Co_3O_4@δ-MnO_2/Pt electrode at the initial state and discharged/recharged to 2.2 V/4.3 V

Table 1 Fitting results of the Nyquist plots using the equivalent circuit

Sample	R_e / Ω	R_f / Ω	Q_1		R_{ct} / Ω	Q_2	
			Y	n		Y	n
Initial	81.9	135.0	3.4×10^{-5}	0.73	331.9	1.8×10^{-5}	0.84
After discharge	89.1	178.1	3.0×10^{-6}	0.61	767.1	3.1×10^{-6}	0.89
After recharge	114.8	162.8	6.7×10^{-5}	0.28	301.6	5.9×10^{-6}	0.92

3 Conclusions

In summary, we propose a unique design of a core-shell Co_3O_4@δ-MnO_2/Pt arrays-type electrode with a controllable, facile route. In this design, the array-type structure facilitates the electrode wetting and oxygen gas transport and supplies free volume for Li_2O_2 loading. The presence of Pt supplies the

catalytically active centers and guides the conformal growth of thin-layered Li_2O_2. The conformal, thin-layered growth of Li_2O_2 on Co_3O_4@δ-MnO_2/Pt enables its easy decomposition upon charge. The porous structure of δ-MnO_2 makes high Li_2O_2 loading possible even though it has a conformal growth mode. As a result, Li-O_2 cell catalyzed by Co_3O_4@δ-MnO_2/Pt arrays delivers high discharge capacity (2 480 mAh·g^{-1} at 100 mA·g^{-1}) and shows good cycling stability (65 cycles at 200 mA·g^{-1} with a limited capacity of 500 mAh·g^{-1}). This work provides a new design of efficient catalytic cathode for Li-O_2 cells.

Supporting information is available at http://www.wjhxxb.cn

References:

[1] Abraham K M, Jiang Z. *J. Electrochem. Soc.*, **1996**,143(1):1-5

[2] Ogasawara T, Débart A, Holzapfel M, et al. *J. Am. Chem. Soc.*, **2006**,**128**(4):1390-1393

[3] Girishkumar G, McCloskey B, Luntz A C, et al. *J. Phys. Chem. Lett.*, **2010**,**1**(14):2193-2203

[4] Park M, Sun H, Lee H, et al. *Adv. Energy Mater.*, **2012**,**2**(7):780-800

[5] Bruce P G, Freunberger S A, Hardwick L J, et al. *Nat. Mater.*, **2012**,**11**(1):19-29

[6] Luntz A C, McCloskey B D. *Chem. Rev.*, **2014**,**114**(23):11721-11750

[7] Aurbach D, McCloskey B D, Nazar L F, et al. *Nat. Energy*, **2016**,**1**:16128

[8] Geng D S, Ding N, Hor T S A, et al. *Adv. Energy Mater.*, **2016**,**6**(9):UNSP 1502164

[9] Yi J, Guo S H, He P, et al. *Energy Environ. Sci.*, **2017**,**10**(4):860-884

[10]Feng N N, He P, Zhou H S. *Adv. Energy Mater.*, **2016**,**6**(9):1502303

[11]Viswanathan V, Thygesen K S, Hummelshj J S, et al. *J. Chem. Phys.*, **2011**,**135**(21):214704

[12]Gerbig O, Merkle R, Maier J. *Adv. Mater.*, **2013**,**25**(22):3129-3133

[13]Shao Y Y, Ding F, Xiao J, et al. *Adv. Funct. Mater.*, **2013**,**23**(8):987-1004

[14]YANG Feng-Yu(杨凤玉), ZHANG Lei-Lei(张蕾蕾), XU Jie-Jing(徐吉静), et al. *Chinese J. Inorg. Chem.*(无机化学学报), **2013**,**29**(8):1563-1573

[15]Chang Z W, Xu J J, Liu Q C, et al. *Adv. Energy Mater.*, **2015**,**5**(21):1500633

[16]Ma Z, Yuan X X, Li L, et al. *Energy Environ. Sci.*, **2015**,**8**(8):2144-2198

[17]Wen Z Y, Shen C, Lu Y. *ChemPlusChem*, **2015**,**80**(2):270-287

[18]Mitchell R R, Gallant B M, Thompson C V, et al. *Energy Environ. Sci.*, **2011**,**4**(8):2952-2958

[19]Jung H G, Hassoun J, Park J B, et al. *Nat. Chem.*, **2012**,**4**(7):579-585

[20]Zhang M, Xu Q, Sang L, et al. *Chin. Sci. Bull.*, **2014**,**59**(24):2973-2979

[21]Guo Z Y, Zhou D D, Dong X L, et al. *Adv. Mater.*, **2013**,**25**(39):5668-5672

[22]Yu M Z, Zhou S, Liu Y, et al. *Sci. China Mater.*, **2017**,**60**(5):415-426

[23]Liu T, Leskes M, Yu W J, et al. *Science*, **2015**,**350**(6260):530-533

[24]McCloskey B D, Speidel A, Scheffler R, et al. *J. Phys. Chem. Lett.*, **2012**,**3**(8):997-1001

[25]Ottakam Thotiyl M M, Freunberger S A, Peng Z Q, et al. *J. Am. Chem. Soc.*, **2013**,**135**(1):494-500

[26]Lu Y C, Xu Z C, Gasteiger H A, et al. *J. Am. Chem. Soc.*, **2010**,**132**(35):12170-12171

[27]Peng Z Q, Freunberger S A, Chen Y H, et al. *Science*, **2012**,**337**(6094):563-566

[28]Xu J J, Wang Z L, Xu D, et al. *Nat. Commun.*, **2013**,**4**:2438(10 Pages)

[29]Li C C, Zhang W Y, Ang H X, et al. *J. Mater. Chem. A*, **2014**,**2**(27):10676-10681

[30]Sun B, Chen S Q, Liu H, et al. *Adv. Funct. Mater.*, **2015**,**25**(28):4436-4444

[31]Jeong Y S, Park J B, Jung H G, et al. *Nano Lett.*, **2015**,**15**(7):4261-4268

[32]Luo W B, Gao X W, Chou S L, et al. *Adv. Mater.*, **2015**,**27**(43):6862-6869

[33]Jiang J, He P, Tong S F, et al. *NPG Asia Mater.*, **2016**,**8**:e239(7 Pages)

[34]Cao Y, Wei Z K, He J, et al. *Energy Environ. Sci.*, **2012**,**5**(12):9765-9768

[35]Hu X F, Han X P, Hu Y X, et al. *Nanoscale*, **2014**,**6**(7):3522-3525

[36]Hu Y X, Zhang T R, Cheng F Y, et al. *Angew. Chem. Int. Ed.*, **2015**,**54**(14):4338-4343

[37]Cui Y M, Wen Z Y, Liu Y. *Energy Environ. Sci.*, **2011**,**4**(11):4727-4734

[38]Black R, Lee J H, Adams B, et al. *Angew. Chem. Int. Ed.*, **2013**,**52**(1):392-396

[39]Wang S F, Sha Y J, Zhu Y L, et al. *J. Mater. Chem. A*, **2015**,**3**(31):16132-16141

[40]Tong S F, Zheng M B, Lu Y, et al. *J. Mater. Chem. A*, **2015**,**3**(31):16177-16182

[41]Liu W M, Gao T T, Yang Y, et al. *Phys. Chem. Chem. Phys.*, **2013**,**15**(38):15806-15810

[42]CAI Sheng-Rong(蔡生容), WANG Xiao-Fei(王晓飞), ZHU Ding(朱丁), et al. *Chinese J. Inorg. Chem.*(无机化学学报), **2016**,**32**(12):2082-2087

[43]Chang Y Q, Dong S M, Ju Y H, et al. *Adv. Sci.*, **2015**,**2**(8):1500092

[44]Liu Q C, Xu J J, Xu D, et al. *Nat. Commun.*, **2015**,**6**:7892 (8 Pages)

[45]Zhao G Y, Mo R W, Wang B Y, et al. *Chem. Mater.*, **2014**,**26**(8):2551-2556

[46]Kim S T, Choi N S, Park S, et al. *Adv. Energy Mater.*, **2015**,**5**(3):1401030

[47]Aetukuri N B, McCloskey B D, García J M, et al. *Nat. Chem.*, **2015**,**7**(1):50-56

[48]Lau S, Archer L A. *Nano Lett.*, **2015**,**15**(9):5995-6002

[49]Radina M D, Siegel D J. *Energy Environ. Sci.*, **2013**,**6**(8):2370-2379

[50]Wang J W, Zhang Y L, Guo L M, et al. *Angew. Chem. Int. Ed.*, **2016**,**55**(17):1-6

[51]Qin Y, Lu J, Du P, et al. *Energy Environ. Sci.*, **2013**,**6**(2):519-531

[52]Wang G Q, Tu F F, Xie J, et al. *Adv. Sci.*, **2016**,**3**(10):1500339

[53]He G Q, Song Y, Liu K, et al. *ACS Catal.*, **2013**,**3**(5):831-838

[54]Song W Q, Poyraz A S, Meng Y T, et al. *Chem. Mater.*, **2014**,**26**(15):4629-4639

[55]Trahey L, Karan N K, Chan M K Y, et al. *Adv. Energy Mater.*, **2013**,**3**(1):75-84

[56]Cao J Y, Liu S Y, Xie J, et al. *ACS Catal.*, **2015**,**5**(1):241-245

[57]Wu F, Zhang X X, Zhao T L, et al. *J. Mater. Chem. A*, **2015**,**3**(34):17620-17626

[58]Zahoor A, Christy M, Kim Y, et al. *J. Solid State Electrochem.*, **2016**,**20**(5):1397-1404

[59]HUANG Jun(黄俊), PENG Zhang-Quan(彭章泉). *Energy Storage Science and Technology*(储能科学与技术), **2018**,**7**(2):167-174

[60]Piao T, Park S M, Doh C H, et al. *J. Electrochem. Soc.*, **2009**,**146**(8):2794-2798